# Control of Grid Connected PV Inverter Acting as STATCOM for Reactive Power Compensation using ANFIS MPPT and Enhanced SPWM.

Paradesi Sowmya [1], Kanna Bhaskar [2]
[1] *M.Tech (Power Electronics) Scholar, Department of Electrical and Electronics Engineering, JNTU Hyderabad, India.*
[2] *Professor, Department of Electrical and Electronics Engineering, JNTU Hyderabad, India.*

***Abstract***: *This paper analyses a grid-connected photovoltaic (PV) inverter system with a dual-stage control framework to enhance energy efficiency and grid compatibility. A MATLAB/Simulink model is developed to evaluate the system's performance, incorporating a Single-Ended Primary Inductor Converter (SEPIC) for optimized energy transfer. The system uses an Adaptive Neuro-Fuzzy Inference System (ANFIS) for improved Maximum Power Point Tracking (MPPT), providing faster convergence and reduced steady state oscillations. The inverter employs an enhanced Sinusoidal Pulse Width Modulation (SPWM) technique, minimizing Total Harmonic Distortion (THD) compared to conventional space vector PWM. Grid Synchronization and regulation of the AC current are achieved through Phase-Locked Loop (PLL), ensuring precise phase and frequency alignment. Simulation results validate the system's stability, rapid dynamic response and effective energy harvesting.*

***Keywords:*** *SEPIC, ANFIS, STATCOM, Enhanced SPWM, LCL filter, PLL.*

## 1. Introduction

The increasing reliance on fossil fuels, which significantly contribute to environmental degradation, underscores the pressing need for renewable energy sources. Solar power, is playing a pivotal role in the transition toward a sustainable energy future, reducing greenhouse gas emissions with a resilient and adaptive energy infrastructure.

The growing global energy demand and population expansion has led the power generation facilities being located far from consumption centres, necessitating extensive transmission networks. These alternating current (AC) systems operating at varying voltage levels, can introduce reliability and stability challenges in interconnected grids. To address these issues, integrating AC/DC and DC/AC converters has become a viable solution.

FACTS devices, using high-speed switching semiconductors, improve AC grid stability, efficiency, and controllability. These devices, typically voltage source inverters (VSIs) synchronized with the system frequency, enable dynamic control to optimize grid reliability and performance. Solar PV systems provide less inherent system stability and reactive power support as they lack rotational inertial unlike conventional synchronous generators. So, they are connected to grid through inverter.

In this paper PV inverter acting like STATCOM is analyzed. The Static Synchronous Compensator (STATCOM), a shunt controller, regulates active and reactive power, ensuring voltage stability across the transmission system. Integrating STATCOM with photovoltaic (PV) systems offers substantial advantages in enhancing grid stability and voltage regulation. The PV array coupled with a DC-DC converter provides a stable and regulated output to the STATCOM, improving power quality.

The transfer of power from the PV array to the Grid is facilitated through DC-DC and DC- AC conversion stages. For this, [1, 2] a two-stage control approach is employed, utilizing current loop regulation for precise voltage and power control to the inverter, enabling efficient grid integration. [3] The inverter switching is achieved using an enhanced Sinusoidal Pulse Width Modulation (SPWM) technique since Space Vector Pulse Width Modulation (SVPWM) is more complex and computationally demanding, particularly in digital implementations. This provides similar modulating waves comparable to conventional SVPWM. Furthermore, the SEPIC DC-DC converter is operated using an ANFIS for MPPT, optimizing the system's efficiency under varying irradiance and temperature conditions [4-6]. This dynamic adjustment of the converter's duty cycle ensures stable DC voltage, which is fed to the STATCOM, further enhancing grid stability and improving power quality.

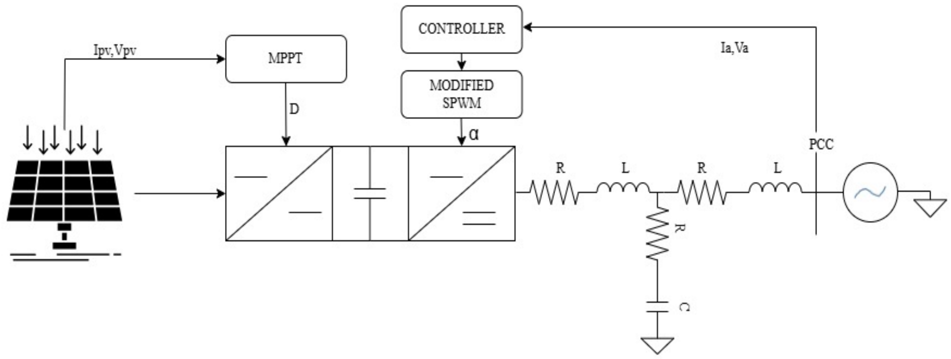


**Figure 1. Single line diagram of Grid Connected PV STATCOM**

Figure (1) shows the single line diagram of the proposed system which shows the two stage conversion i.e. DC-DC conversion and AC-DC conversion. An LCL filter is used between the inverter and grid to minimize harmonic content, ensuring a clean sinusoidal waveform.

## 2. Methodology

The photovoltaic (PV) system generates DC voltage from solar energy, which is adjusted to the required level through a DC-DC converter controlled by an ANFIS. The regulated DC voltage is then converted into AC using a grid-connected inverter with enhanced SPWM. To ensure high-quality power, the AC output is filtered through an LCL filter to minimize harmonics before being synchronized with the grid for efficient integration. This process is carried out in two stages: DC-DC conversion with ANFIS control and DC-AC conversion with enhanced SPWM. For simplification the two stage converter is analyzed in dq reference frame using park's transformation.

### 2.1. ANFIS based MPPT control of DC-DC Converter:

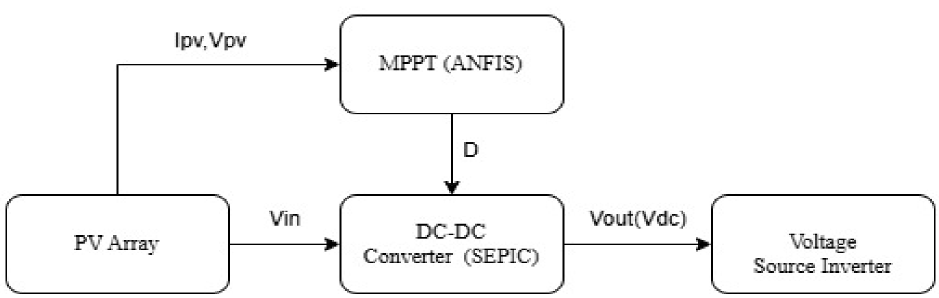


**Figure 2. Block Diagram for DC-DC Conversion.**

Figure (2) shows the block diagram of dc-dc conversion stage. This stage manages PV operating point by adjusting its input voltage and current. As the stabilization of dc link voltage of the inverter is vital for smooth operation, the SEPIC is chosen for its capability as both step up or step down converter, making it highly suitable for application with wide input voltage variations found in PV systems.

**2.1.1. Designing of SEPIC Converter:**

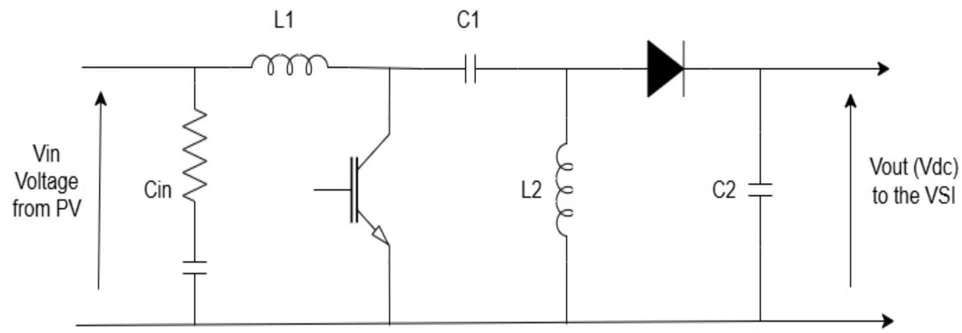


**Figure 3. SEPIC Converter**

Figure (3) shows the diagram of SEPIC converter. The dc input is given from the PV and duty cycle by the ANFIS controller. L1 is the inductor at the input and L2 is the inductor at the output. C1 and C2 are the coupling and output capacitors respectively [12]. These parameters are calculated using the equations (1-3).

**1. Duty Cycle:**

$$D = \frac{V_o}{V_o+V_{in}} \tag{1}$$

Where $V_o$ is output voltage,
$V_{in}$ is input voltage.

**2. Inductor L1, L2:**

$$L1=L2= \frac{V_{g(\min)}*D_{max}}{2*\Delta IL*f_{sw}} \tag{2}$$

Where $\Delta IL$ = 40% * $I_{in}$

$$I_{in}= \frac{I_{out}*V_o}{V_{in}}$$

$D_{max}$= maximum duty cycle,
$f_{sw}$ is switching frequency,
$I_{in}$ is input current,
$I_{out}$ is output current.

**3. Output Capacitor**

$$C_2 > \frac{I_{out}*D_{max}}{C_s*f} \tag{3}$$

The duty cycle of the SEPIC converter is dynamically modulated in response to the changes in the irradiance and temperature for maintaining consistent dc link voltage. Dynamic adjustment and adaptive approach of duty cycle ensures near optimal power extraction, enhancing system stability and maintain a robust DC link voltage. This is essential for efficient power injection into the grid and maintaining a reliable connection in the second stage.

Advanced hybrid methods like ANFIS optimize the duty cycle to ensure operation at the Maximum Power Point (MPP).

### 2.1.2 ANFIS MPPT:

The ANFIS integrates the learning capabilities of neural networks with the reasoning capabilities of fuzzy logic. This combination is a powerful tool for control, forecasting, and modelling of complex systems like photovoltaic systems. Neural networks utilize statistical training, while fuzzy logic incorporates expert knowledge. By leveraging both, ANFIS constructs through a hybrid algorithm that combines the least squares method with the back propagation gradient approach.
The ANFIS controller training process involves generating data set by varying operating temperature and solar irradiance levels. The ANFIS model is designed with two inputs irradiance and temperature to produce a control signal, which serves as the reference voltage. This reference voltage is compared with the actual PV voltage and the resulting error is processed by proportional integral controller to adjust the duty cycle of the SEPIC converter.

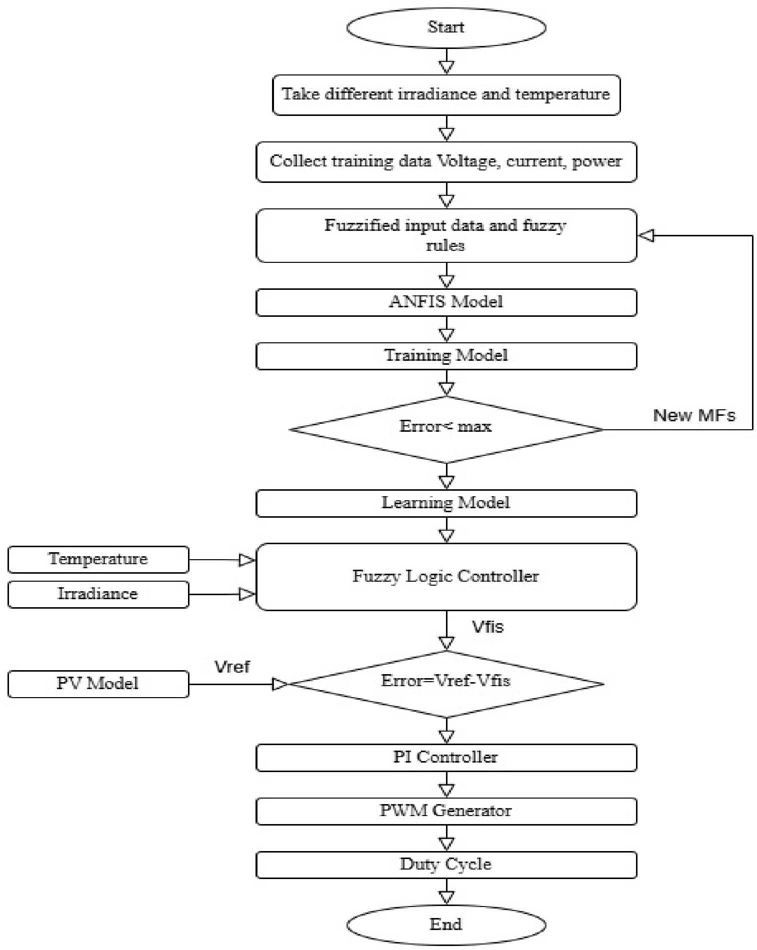


**Figure 4. Flow chart of ANFIS**

The flowchart illustrating the execution of the ANFIS-based maximum power point tracking is shown in figure (4).
In this only voltage (Vfis) is considered. This is calculated using the equation

$$V_{fis} = V_{pp} + ß * (\mathrm{T} - T_s)) + \alpha * (1 + \frac{G}{G_s}) \tag{4}$$

Where Ts=25°C and Gs=1000 w/$m^2$

Once the system converges to the optimal point, the duty cycle stabilizes and remains constant until environmental variations necessitate a re-evaluation. In the absence of MPPT adjustment, fluctuations in the PV input could lead to instability in the DC-DC converter output, adversely affecting the inverter's performance.

To ensure proper DC link voltage regulation, a reference value of 800 V is maintained. This reference voltage ensures the DC link remains stable at the inverter stage, even under varying environmental conditions. A capacitor integrated into the DC link mitigates voltage fluctuations and provides a stable energy buffer, supporting efficient operation of the inverter and improved overall system performance.

### 2.2 VSI driven by Enhanced SPWM:

The regulated dc voltage from the dc-dc converter is supplied to the inverter. The voltage source inverter converts DC- AC. These currents are utilized to derive the reference inverter currents ($I_d^*$) for the PI controller. It regulates the inverter's output to match the desired reference AC voltage. The PI controller adjusts both the modulation index and phase of the output AC signal to maintain synchronization with the grid. It compares the actual AC voltage from the Voltage Source Inverter (VSI) ($V_d', V_Q'$) with the grid reference voltage ($V_d, V_q$) and corrects any discrepancies, ensuring the inverter's output meets the required voltage, frequency, and phase specifications. which are then used to obtained voltages ($V_d^*, V_q^*$) in dq reference frame. These voltages get added with the cross coupling terms (wL$i_d$, wL$i_q$) and produce reference voltages ($V_d^*, V_q^*$) which are subsequently transformed into three phase reference signals using inverse Park's transformation. These signals are used to produce switching pulses for the voltage source inverter (VSI) using enhanced SPWM technique to ensure efficient DC-AC conversion.

The figure (5) shows the schematic of the current controller. The control of real and reactive power depends on d-axis current component and q- axis current component respectively. The active and reactive power equations in synchronous reference frame are given in (5-7).

$$P = \frac{3}{2}(V_d I_d + V_q I_{q)} = \frac{3}{2}(V_d I_d) \tag{5}$$

$$Q = \frac{3}{2}(V_d I_q - V_q I_{d)} = \frac{3}{2}(V_d I_q) \tag{6}$$

$$I_q^* = \frac{2Q^*}{3V_d} \tag{7}$$

Synchronization of the inverter's output frequency and phase with the grid is critical to ensure proper integration. This synchronization is achieved using a Phase-Locked Loop (PLL), which maintains precise alignment between the inverter and grid voltages. Effective Synchronization facilitates seamless power transfer and prevents power quality issues, such as harmonic distortion or phase misalignment, which could adversely impact grid stability and operation.

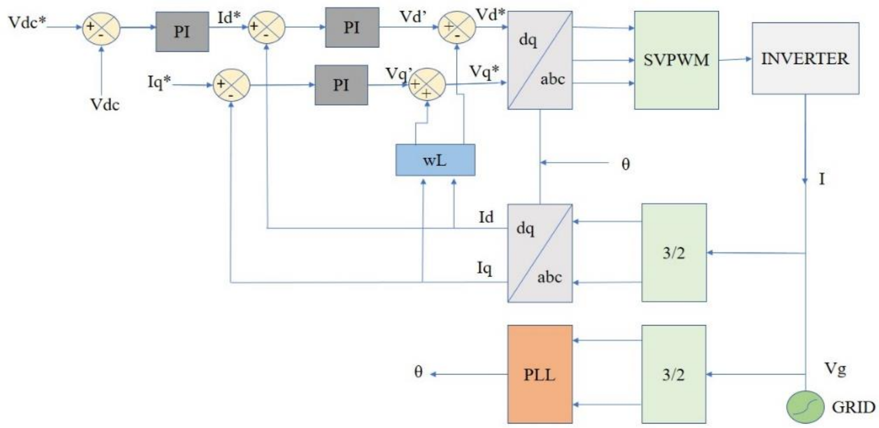


**Figure 5. Schematic of Current Controller**

### 2.2.1 Controller Equations

$$V_{i,a} - V_{g,a} = L\frac{di_a}{dt} + Ri_a \tag{8}$$

Where $V_{i,a}, V_{i,b}$ are output voltages of the inverter and the grid respectively in three phase.
$i_a$ is the inverter output current in three phase.
Applying dq transformation to current derivation,
Due to rotation of the dq frame the time derivative of the dq transformed form of the $i_d$ or $i_q$ is given as

$$\frac{d}{dt}\begin{bmatrix} i_d \\ i_q \end{bmatrix} = \begin{bmatrix} i_d^* \\ i_q^* \end{bmatrix} + w\begin{bmatrix} 0 & -1 \\ 1 & 0 \end{bmatrix}\begin{bmatrix} i_d \\ i_q \end{bmatrix} = \begin{bmatrix} i_d^* - wi_d \\ i_q^* + wi_q \end{bmatrix} \tag{9}$$

Where w= angular frequency. It is obtained using PLL.
wL$i_d$, wL$i_q$ = cross coupling terms. These are introduced due to rotation of frame.

$$V_{i,d} - V_{g,d} = L\frac{di_d}{dt} - \mathrm{wL}i_d + Ri_d \tag{10}$$

$$V_{i,q} - V_{g,q} = L\frac{di_q}{dt} + \mathrm{wL}i_q + Ri_q \tag{11}$$

Final equations for obtaining $V_d, V_q$ are given as

$$V_{i,d} = L\frac{di_d}{dt} - \mathrm{wL}i_d + Ri_a + V_{g,d} \tag{12}$$

$$V_{i,q} = L\frac{di_q}{dt} + \mathrm{wL}i_q + Ri_q + V_{g,q} \tag{13}$$

Where $V_{i,d}, V_{i,q}$ are the inverter output voltages in the dq frame.
$V_{g,d}, V_{g,q}$ are the grid voltages in the dq frame.
$i_d, i_q$ are the inverter output currents, regulated by the inverter's control system to manage the power flow between the PV system and the grid.

### 2.2.2. Enhanced SPWM

The figure (6) shows the block representation of the implemented voltage modulation for the inverter. In Conventional Space Vector Pulse Width Modulation (SPVWM), the three phase voltages or currents are transformed into voltage space vectors using space vector transformation. These voltage space vectors serve as reference despite three phase modulating waves. This process is computationally intensive and complex. For obtaining these space vectors, the sectors must be identified by applying active vector, switching sequences are determined based on the sector in which the sample reference vector resides. Even when the reference vector falls within the sector, adjustments for forward and reverse switching sequences are need. Additionally, the calculation of the dwell times involves trigonometric functions and loop up tables, further increasing the computational burden. These complexities can be mitigated by adopting an enhanced approach where the voltage vectors are derived using a common mode component.

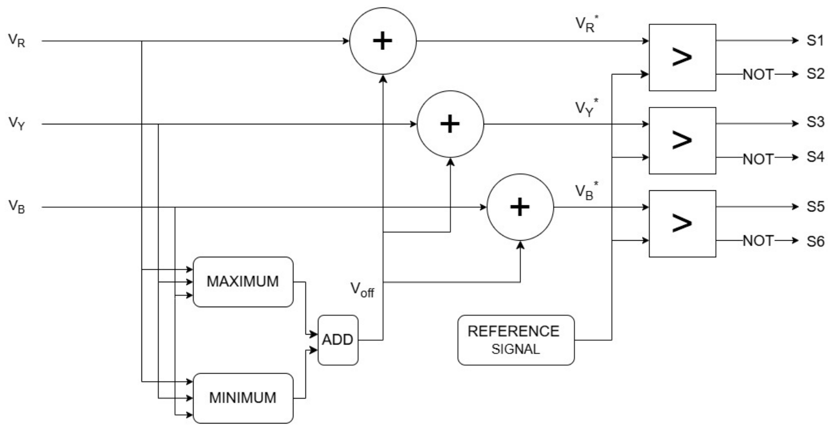


**Figure 6. Enhanced SPWM**

This common mode component resembles a triangular wave with peak of 0.25Vm. Addition of this common mode component ($V_{off}$) to modulating signal of each phase ($V_R, V_Y, V_B$) results in modified modulating signal ($V_R^*, V_Y^*, V_B^*$) which produces waveforms similar to those generated using CSVPWM.

$$V_{off} = -0.5(V_{max} + V_{min}) \tag{14}$$

$$(V_R^*, V_Y^*, V_B^*) = (V_R, V_Y, V_B) + (V_{off}, V_{off}, V_{off}) \tag{15}$$

Equation (14) calculates the offset voltage, while equation (15) defines the modified voltage references.

## 3. Simulation Diagram:

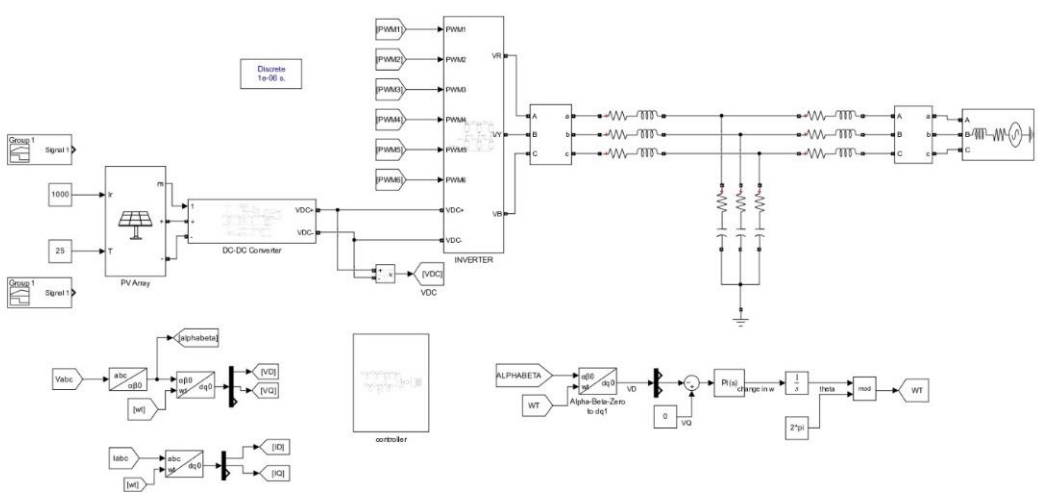


**Figure 7. Simulation Model of the Proposed System**

Figure (7) shows the simulation model of the proposed system which includes the DC-DC converter, DC-AC converter controlled with ANFIS MPPT and current controller respectively along with abc to dq transformation and PLL.

**Table 1. Specifications of PV Module**

| Parameter | Value |
|---|---|
| Maximum Power | 213.15(Pmax) |
| Cells per Module | 60 |
| Open Circuit Voltage | 36.3(Voc) |
| Short circuit current | 7.84(Isc) |
| Voltage at maximum power point | 29(Vpp) |
| Current at maximum power point | 7.35(Ipp) |
| Temperature coefficient of Voc | -0.36099(ß) |
| Temperature coefficient of Isc | 0.102(α) |

**Table 2. Parameter Values for Grid**

| Parameter | VALUE |
|---|---|
| Total Power | 100KW |
| Grid voltage | 415V |
| Frequency | 50Hz |

**Table 3. Parameter Values of SEPIC Converter**

| Parameter | Value |
|---|---|
| Inductance (L1,L2) | 28.3μH |
| Capacitance | C1=1000μF, C2=4000μF |

Table (1-3) show the parameter values used in the proposed system.

## 4. Results and Discussion:

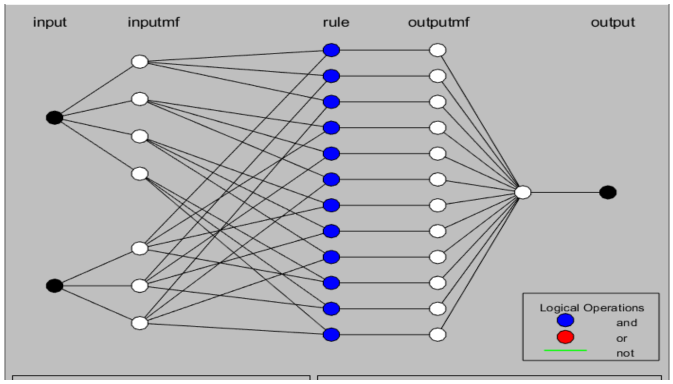


**Figure 8. Structure of 5 layer ANFIS**

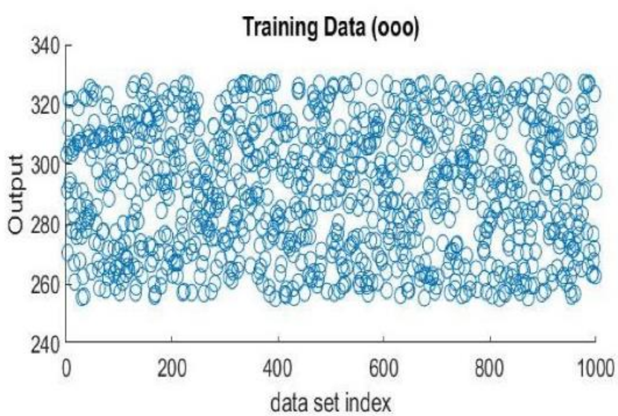


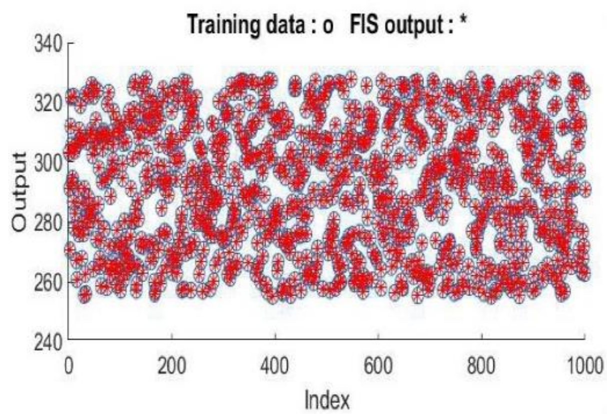


**Figure 9. Training Data of ANFIS**

**Figure 10. FIS output**

In figure (8) structure of ANFIS is shown. Where layer 1 is input layer, layer 2 is rule strength computation layer, layer 3 is Normalization layer, layer 4 is rule output layer and layer 5 is output layer.

To enhance the overall system performance, a comprehensive dataset comprising 1,000 data samples (Figure 9) by varying temperature (Tmin=15°C to Tmax=35°C) and irradiance (Gmin=0w/$m^2$ to Gmax=1000w/$m^2$) is utilized for training the ANFIS model.


**Figure 11. Training Error**

The model undergoes training for 100 epochs using hybrid optimization method with 4,3 membership functions and the fis is tested against the trained data (figure 10) achieving a significant reduction in training error to approximately 0.0004% (figure 11), demonstrating exceptional precision and reliability in the modulation strategy.

### 4.1 VSI driven by Enhanced SPWM:

The Figure (12) shows the waveform of the enhanced SPWM, which includes the modulating signal, the reference sine wave, and the common mode voltage. This waveform highlights the effective modulation technique used to improve the performance and control of the inverter. The modulating signal is compared with the reference sine wave to generate the switching pulses for the inverter.

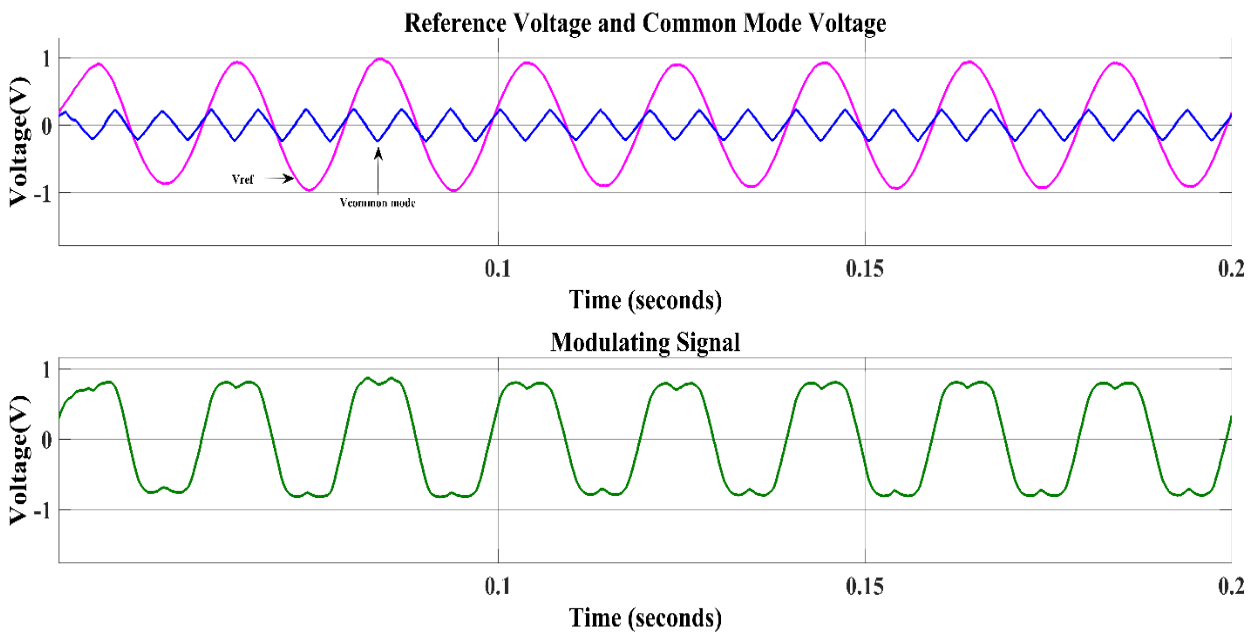


**Figure 12. Enhanced SPWM**

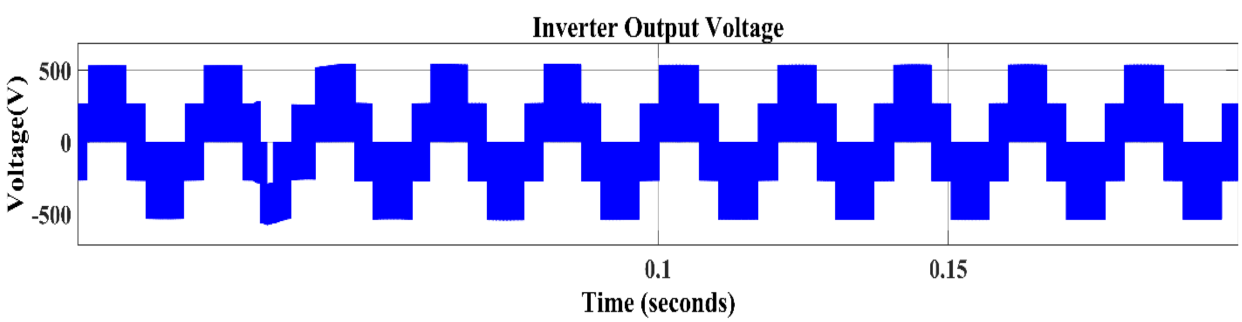


**Figure 13. Output voltage (phase to ground) waveform of the inverter for single phase.**

The figure (14) shows the current before and after passing through the filter. It is evident that the filter effectively reduces the ripple content, resulting in a more sinusoidal current waveform.

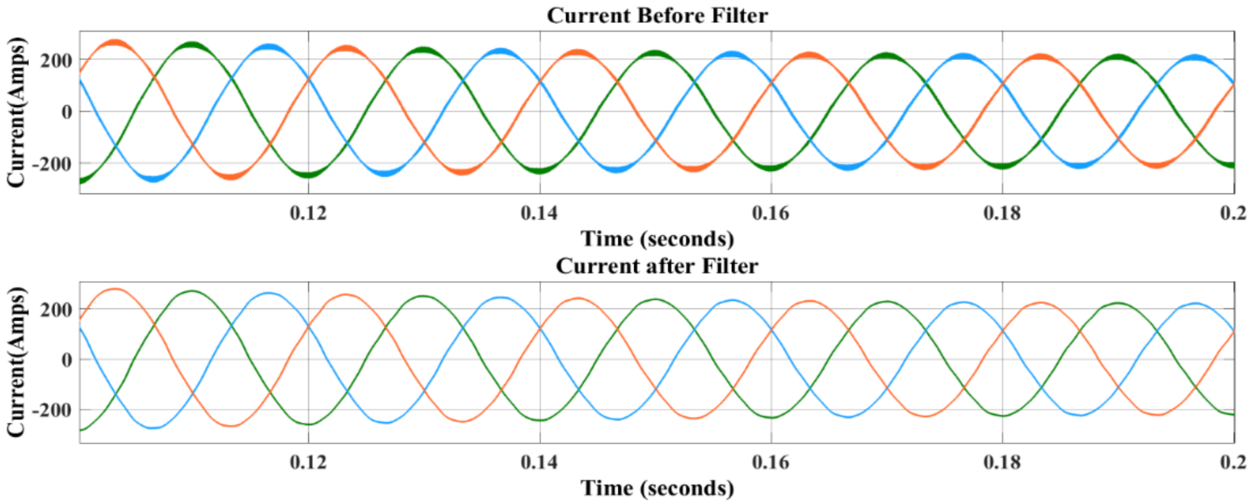


**Figure 14. Current Before and After Filter.**

The Figure (15) shows the THD of the inverter current, which is obtained using the enhanced SPWM technique. The THD is observed to be low, indicating that the enhanced SPWM approach effectively reduces harmonic content in the output current. This reduction in THD contributes to improved performance of the system, enhancing both the quality of the power delivered and the overall efficiency of the inverter

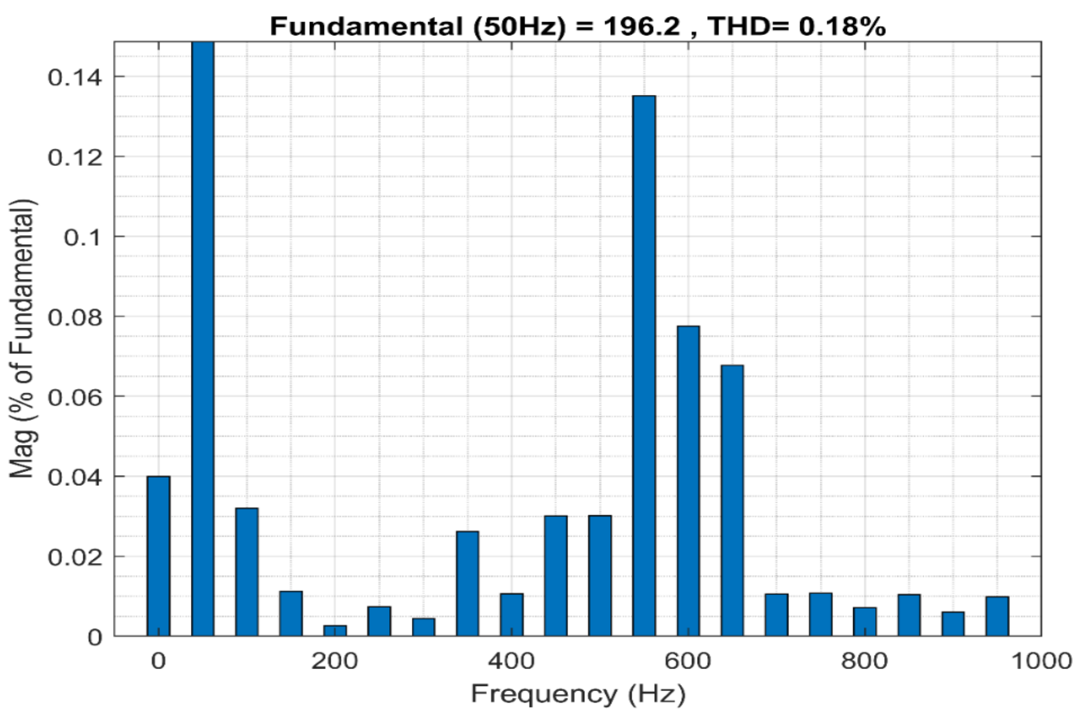


**Figure 15. Total Harmonic Distortion (THD).**

### 4.2 Case 1: At Constant Temperature (25°C) and Irradiance (1000w/$m^2$)

The simulation results are conducted under Standard Test Conditions (STC), defined by an irradiance of 1000 W/m² and a temperature of 25°C. The I-V and P-V curves, shown in Figure (15), offer valuable insights into the performance of the photovoltaic (PV) system and help identify the Maximum Power Point (MPP). System efficiency is assessed by comparing the power output at the Point of Common Coupling (PCC) with the maximum power under STC (figure 16), ensuring the system operates at peak performance. The figure (17) shows power from the solar panel at constant irradiance and temperature under selected PV modules and strings.

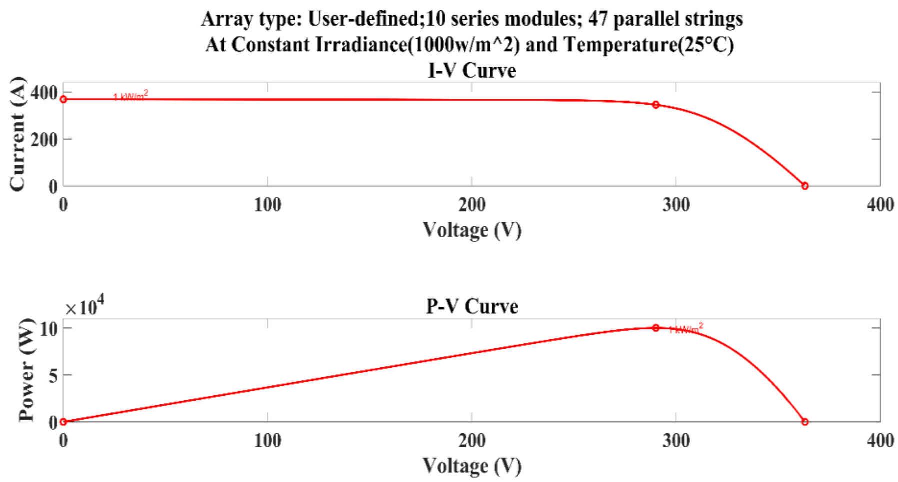


**Figure 16. I-V and P-V Curves at Constant Irradiance (1000w/m^2) and Temperature (25°C).**

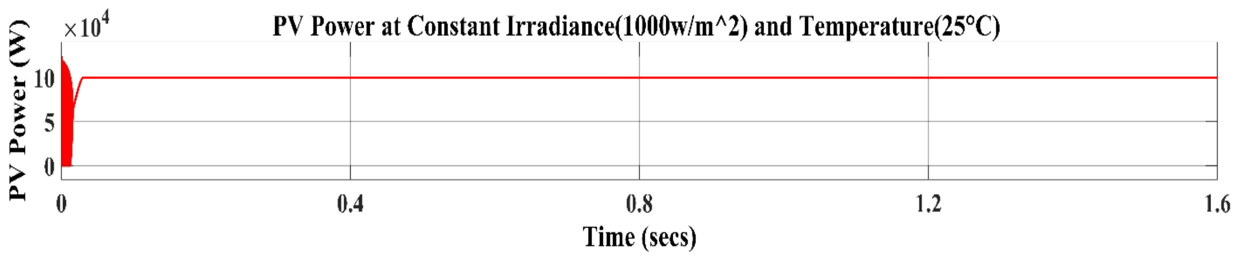


**Figure 17. PV Power at Constant Irradiance (1000w/m^2) and Temperature (25°C).**

Figure (18) illustrates the current, voltage, and power waveforms measured at the Point of Common Coupling (PCC) under the applied irradiance and temperature conditions. The observed power values indicate that the photovoltaic (PV) system operates at its Maximum Power Point (MPP), with the generated power being effectively delivered at the PCC. The following figure (19) shows the duty cycle of the dc to dc converter which is maintained constant throughout under STC.

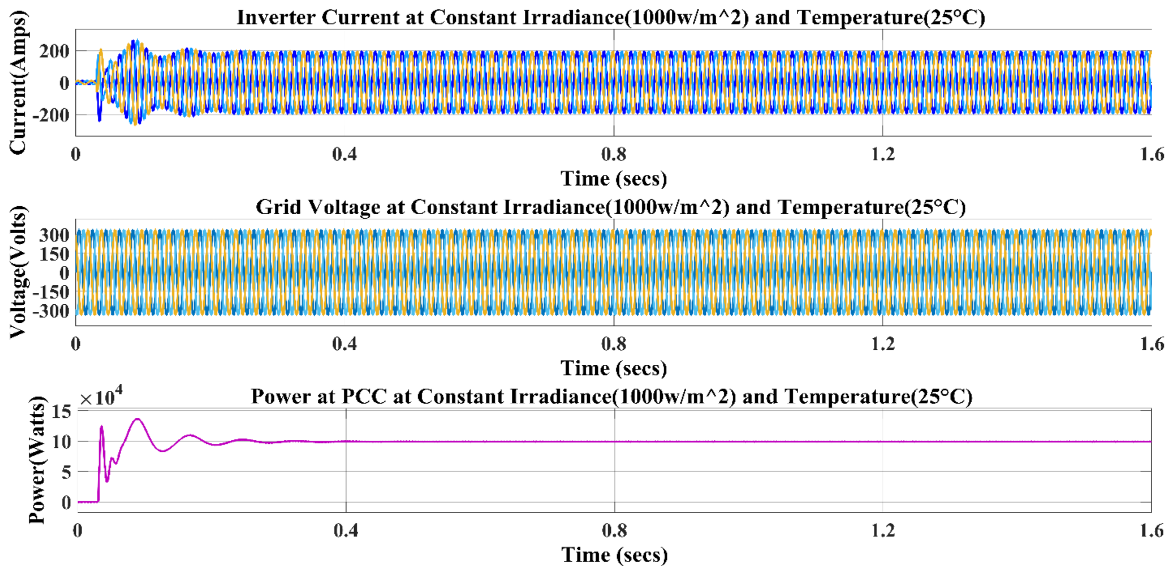


**Figure 18. Inverter Current, Grid Voltage and Power at PCC at Constant Irradiance (1000w/m^2) and Temperature (25°C).**

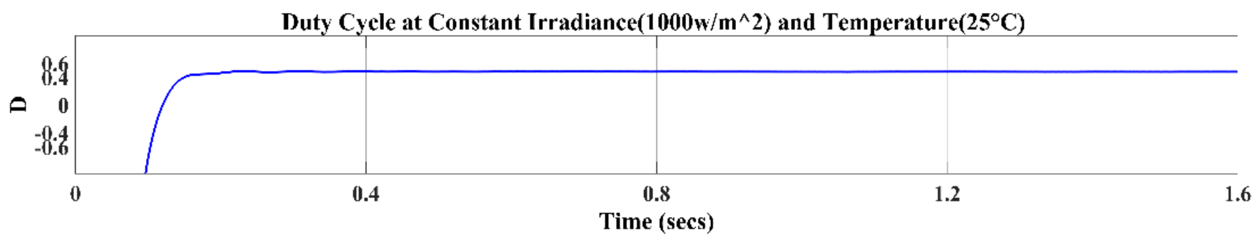


**Figure 19. Duty Cycle at Constant Irradiance (1000w/m^2) and Temperature (25°C).**

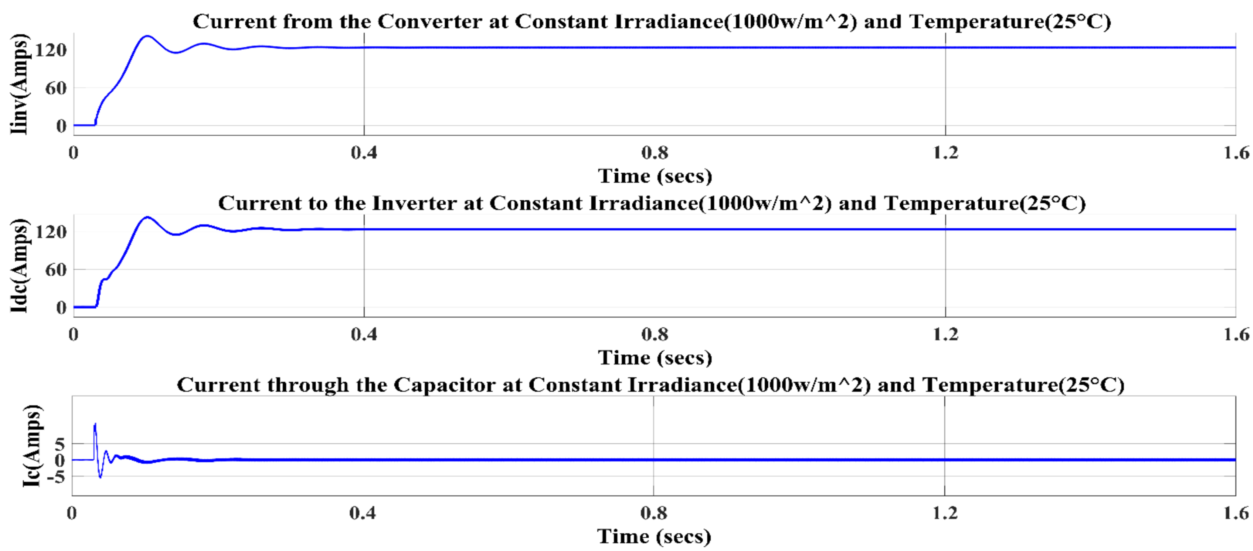


**Figure 20. Currents from the Converter, to the Inverter and through the Capacitor at Constant Irradiance (1000w/m^2) and Temperature (25°C).**

The figure (20) shows the current waveforms at the node where the inverter interfaces with the converter output to achieve the desired DC voltage. The current from the converter, the current to the inverter, and the current through the capacitor, respectively. Analysis of these waveforms indicates that the current flowing through the capacitor is minimal, emphasizing its role in voltage stabilization.

### 4.3 Case 2: For Variation in Irradiance and at Constant Temperature (25°C):

For the dynamic analysis, the system is considered to be exposed to changing irradiance and the temperature is taken constant that is 25°C.

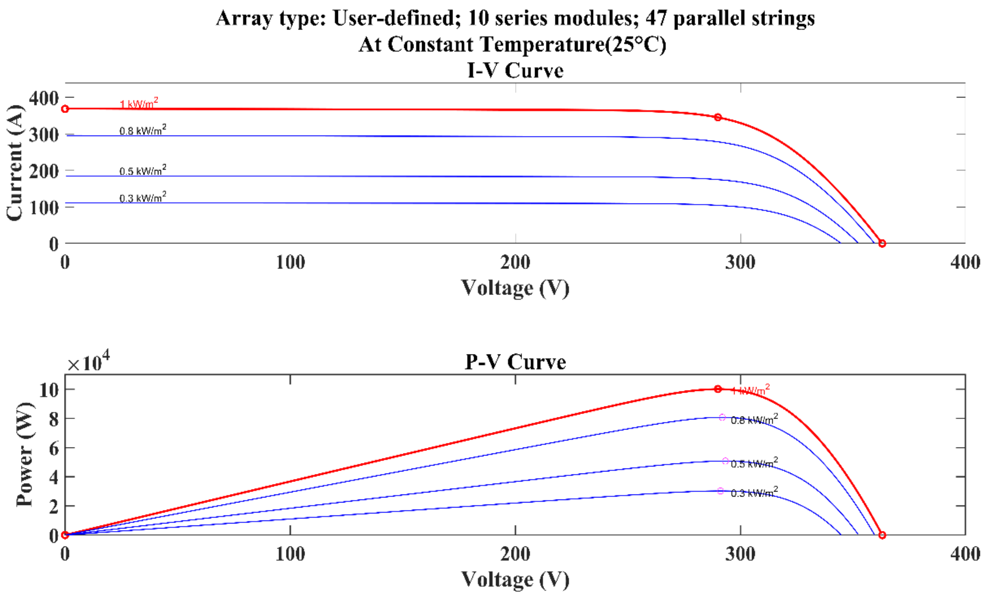


**Figure 21. I-V and P-V Curves at Constant Temperature (25°C).**

The figures (21, 22) show the I-V, P-V Curves and PV Power at Constant Temperature respectively.
In the simulation, the system's irradiance of the system is varied periodically. At t=0 the irradiance is set to 1000w/m^2 resulting in a maximum power output of approximately 100kw from the PV system, with the temperature maintained at 25C. At t=0.4, the irradiance is reduced to 800w/m^2 and the PV system generates a maximum power of 80kw. Subsequently, at t= 0.8, the irradiance is further decreased to 500w/m^2, causing the maximum power output to drop to 50kw. Finally, at t= 1.2, the irradiance is lowered to 300w/m^2, reducing the maximum power output to 30kw.

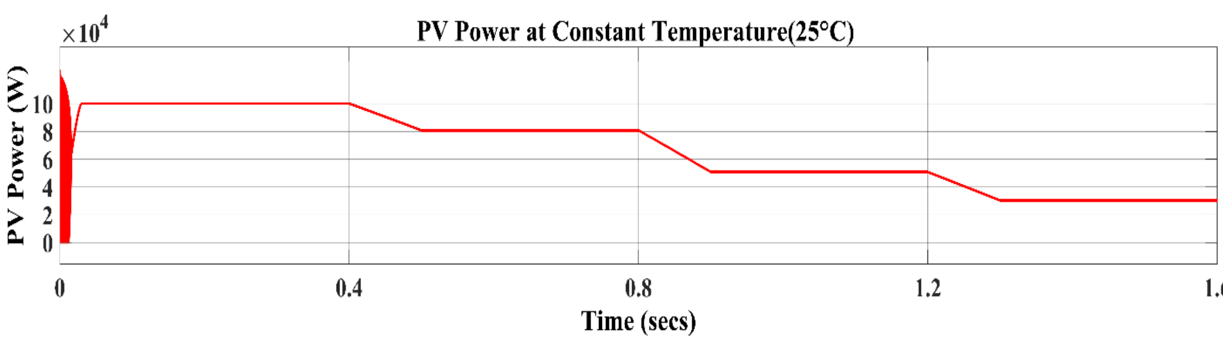


**Figure 22. PV Power at Constant Temperature (25°C).**

As the irradiance changes, the inverter current decreases proportionally, as the current is directly related to the irradiance from the photovoltaic (PV) system. Similarly, the power output from the inverter also decreases with the reduction in irradiance, since power is directly proportional to irradiance. This can be seen from the figure (23)

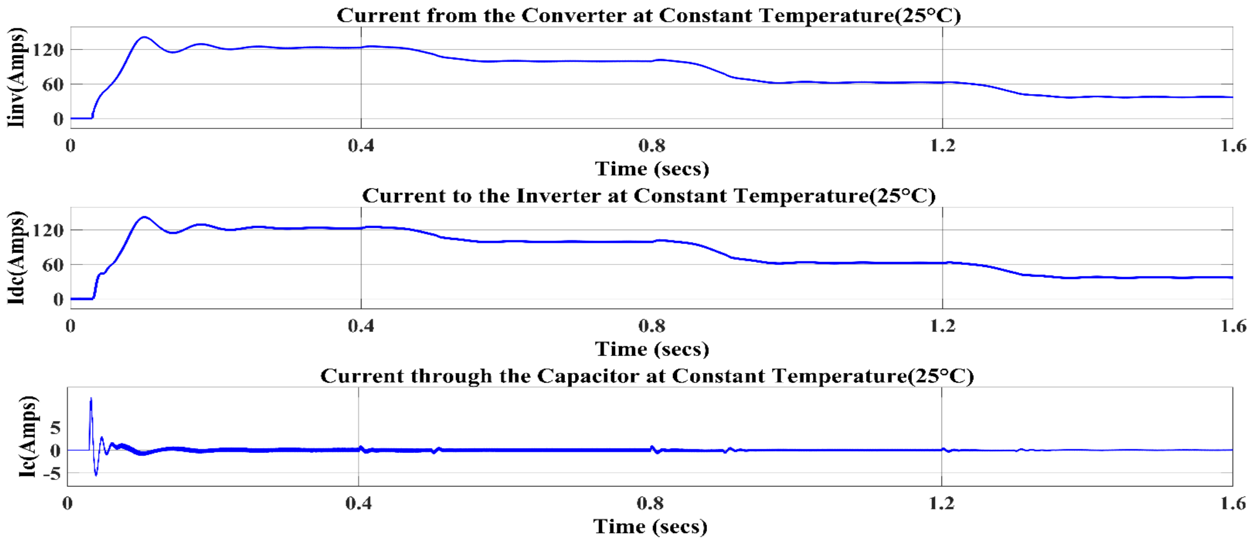


**Figure 23. Inverter Current, Grid Voltage and Power at PCC at Constant Temperature (25°C).**

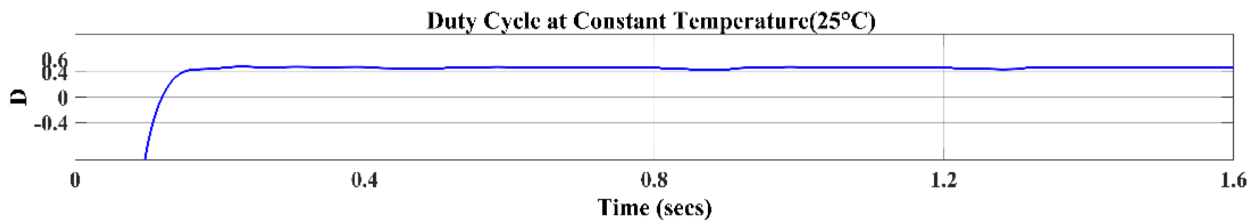


**Figure 24. Duty Cycle at Constant Temperature (25°C).**

The Figure (24) shows the variation in the duty cycle in response to changes in irradiance. As the irradiance decreases, the duty cycle adjusts accordingly and then stabilizes back to its initial value, as observed in the resulting waveform. The figure (25) shows the current through the capacitor, which remains minimal even under varying conditions. This low current through the capacitor is crucial for maximizing the power output while minimizing losses, ensuring efficient power transfer from the photovoltaic (PV) system to the inverter.

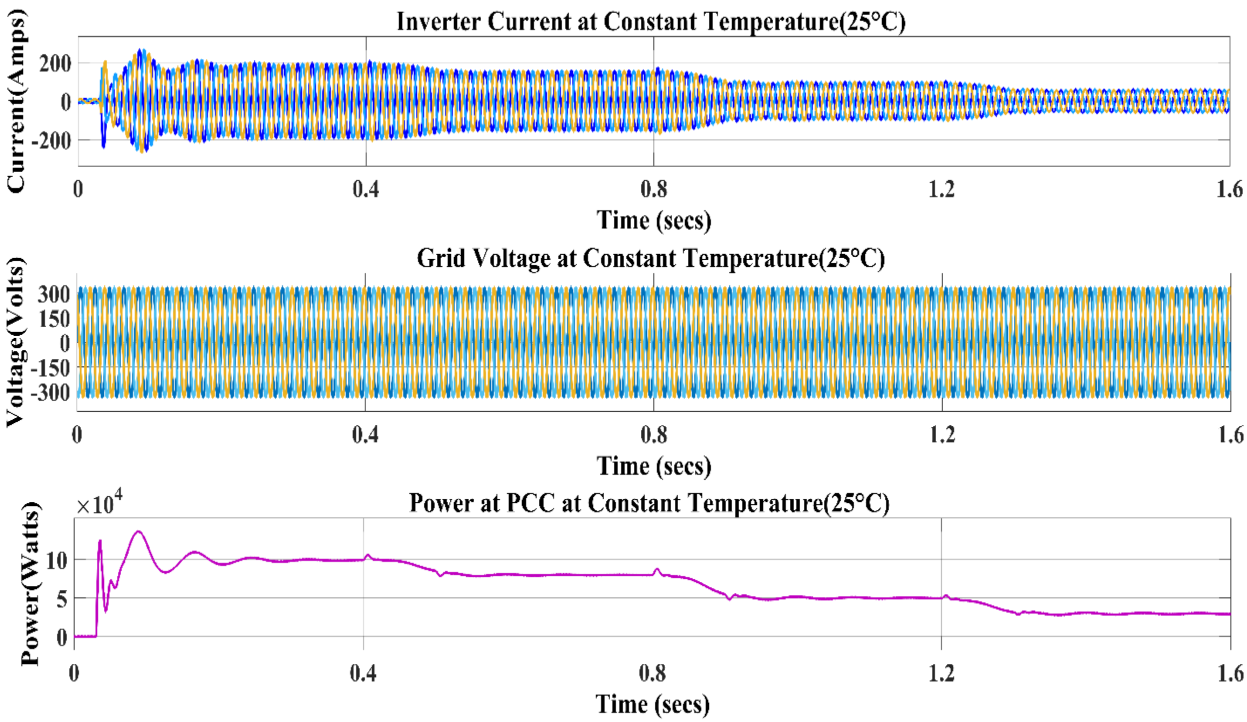


**Figure 25. Currents from the Converter, to the Inverter and through the Capacitor at Constant Temperature (25°C).**

### 4.4 Case 3: At Constant Irradiance and Variable Temperature

A constant irradiance of 1000 W/m² is maintained while the temperature varies over time, with dynamic performance evaluated at t=0.4t = 0.4t=0.4, 0.80.80.8, and 1.21.21.2 seconds.

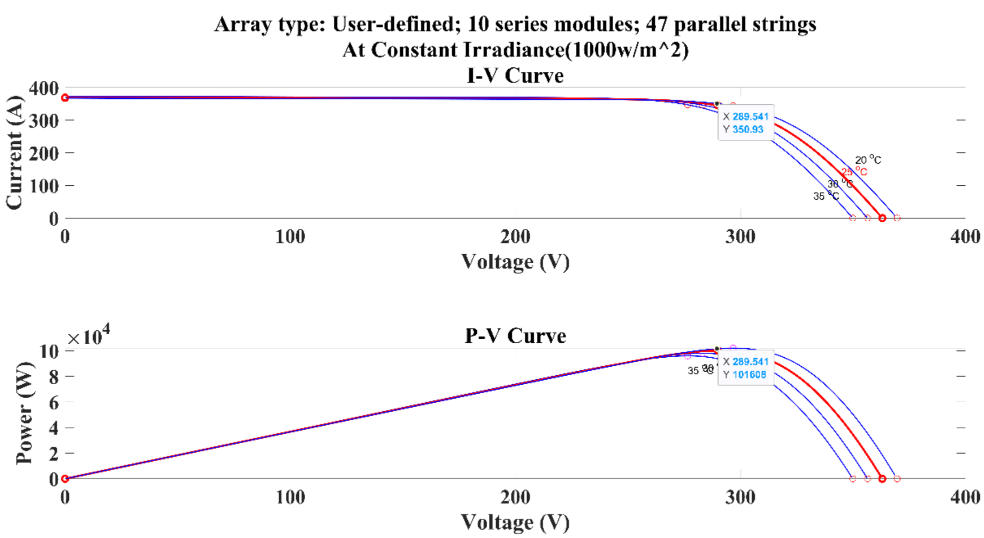


**Figure 26. I-V and P-V Curves at Constant Irradiance (1000w/M^2)**

The I-V and P-V curves for temperature variations are shown in Figure (26), and Figure (27) displays the power output of the PV system. While temperature changes affect the system, their impact on maximum power is minimal compared to irradiance variations. A decrease in temperature leads to a slight increase in power due to improved efficiency and higher open-circuit voltage.

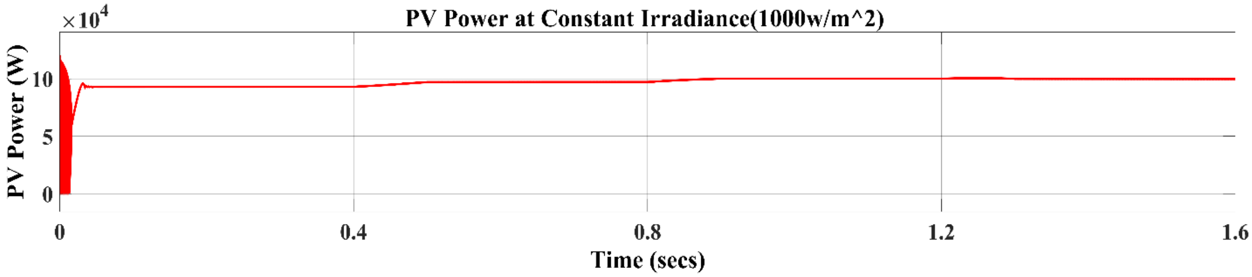


**Figure 27. PV Power at Constant at Constant Irradiance (1000w/m^2).**

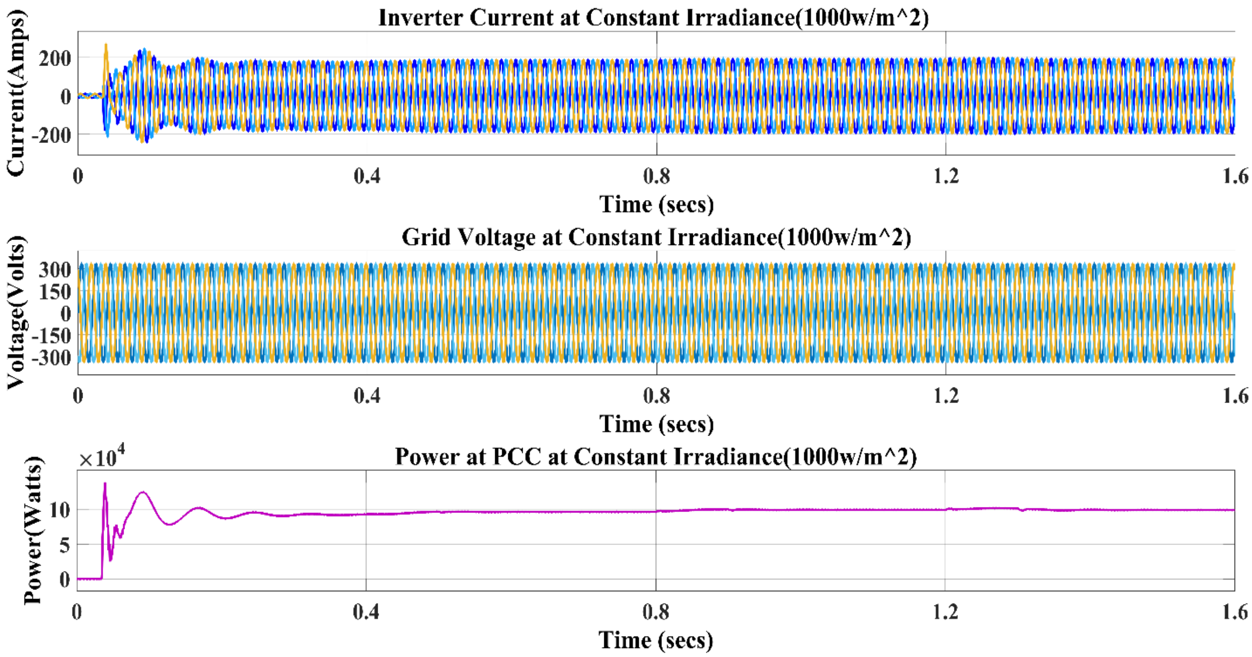


**Figure 28. Inverter Current, Grid Voltage and Power at PCC at Constant Irradiance (1000w/m^2).**

From figure (28), At the Point of Common Coupling (PCC), the power output stays mostly constant, with a slight increase observed as the temperature decreases, while irradiance remains constant. This small increase in power aligns with the inverter current behavior, where temperature variations have minimal effect on the current. The PV system's efficiency improves slightly at lower temperatures, leading to a marginal rise in power output at the PCC.

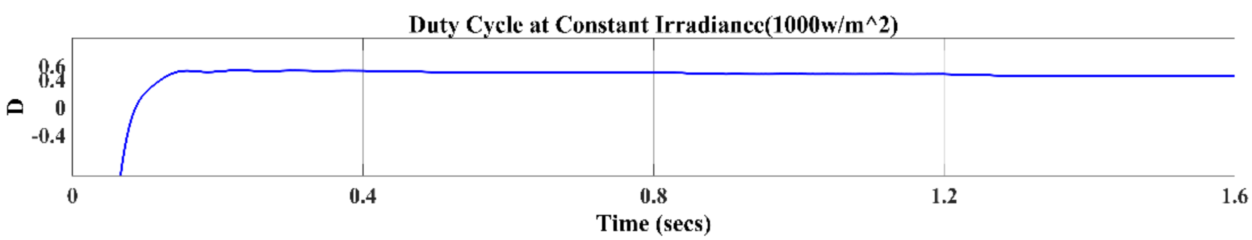


**Figure 29. Duty Cycle at Constant Irradiance (1000w/m^2).**

Figure (29), illustrates the duty cycle under constant irradiance while temperature varies. It is observed that, despite temperature fluctuations, the duty cycle remains stable, adjusting to the conditions and maintaining a steady value as the system compensates for the temperature changes. The figure (30) shows the current flowing through the capacitor. It is observed that the current through the capacitor remains minimal, indicating that the capacitor primarily serves to stabilize the voltage with very little current flow.

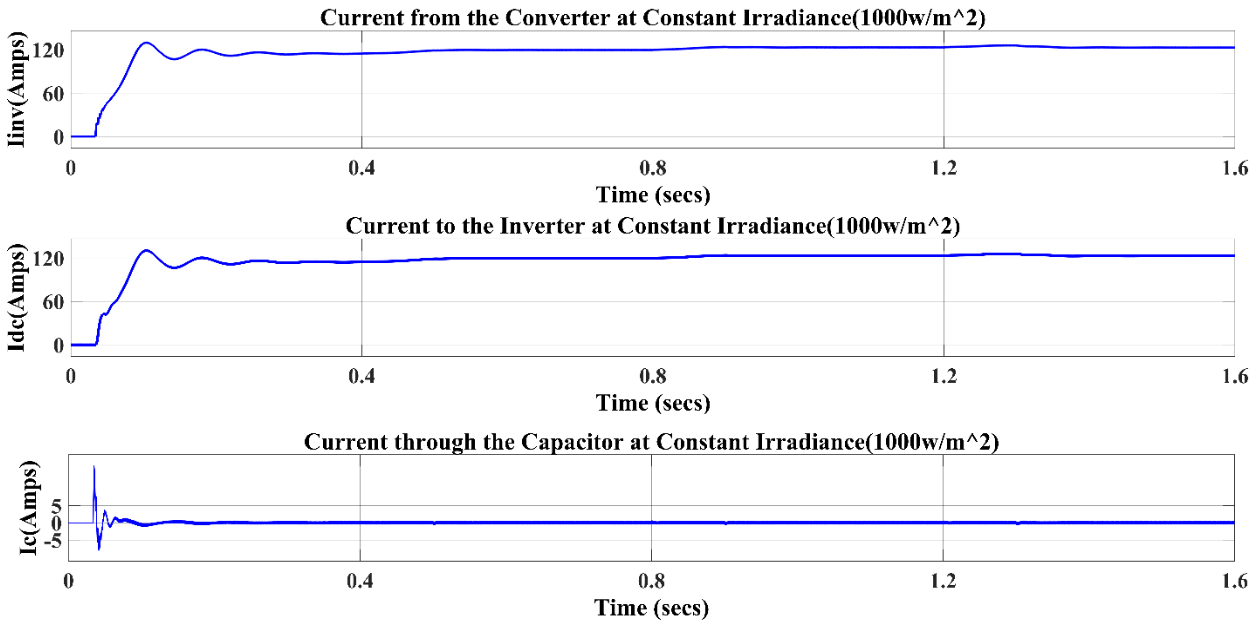


**Figure 30. Currents from the Converter, to the Inverter and through the Capacitor at Constant Irradiance (1000w/m^2).**

**Table 4. Currents at the Capacitor with Change in Temperature**

| | **35** | **30** | **25** | **20** |
|---|---|---|---|---|
| Currents from the Converter | 113.5 | 119.2 | 124 | 126 |
| Currents through the Capacitor | 0.137 | 0.43 | 0.44 | 0.44 |
| Currents to the Inverter | 113.4 | 118.8 | 123.6 | 125.7 |

**Table 5. Currents at the Capacitor with Change in Irradiance**

| | **1000** | **800** | **500** | **300** |
|---|---|---|---|---|
| Currents from the Converter | 131.4 | 111.7 | 77.4 | 45.02 |
| Currents through the Capacitor | 0.45 | 0.31 | 0.44 | 0.089 |
| Currents to the Inverter | 131 | 111.4 | 77.27 | 44.93 |

The loss of a capacitor is typically assessed by calculating its dissipation factor (DF) or equivalent series resistance (ESR), which indicate the amount of energy dissipated as heat. The capacitor with low dissipation factor is preferred as it minimizes voltage drop ensuring that the maximum voltage is delivered to the inverter input. By observing both the tables (4, 5) it can be seen that the current through the capacitor remains low, indicating its role in voltage stabilization. These results demonstrate the system's efficient power transfer with capacitor effectively maintaining voltage regulation.

### 4.5 Case 4: For Diurnal Irradiance and Temperature Variations.

The figure (31) shows, a time scale of 1 hour = 0.067 sec is applied on the x-axis. In the early morning (at t=0 to t=0.4), as sunlight begins to increase, solar irradiance rises, leading to a proportional increase in PV power output. Correspondingly, supported by lower ambient temperatures that optimize module efficiency. Around midday (at t=0.4 to t=0.8), irradiance reaches its peak, resulting in maximum power generation. However, elevated temperatures slightly reduce efficiency due to the negative temperature coefficient of the PV modules. During the afternoon(at t=0.8 to t=1.2), declining irradiance, as the sun descends, becomes the primary factor driving a steady reduction in power output, even as temperatures remain elevated. After sunset (at t=1.2 to t=1.6), with no available irradiance PV power generation ceases entirely and ambient temperature variations no longer impact system performance.

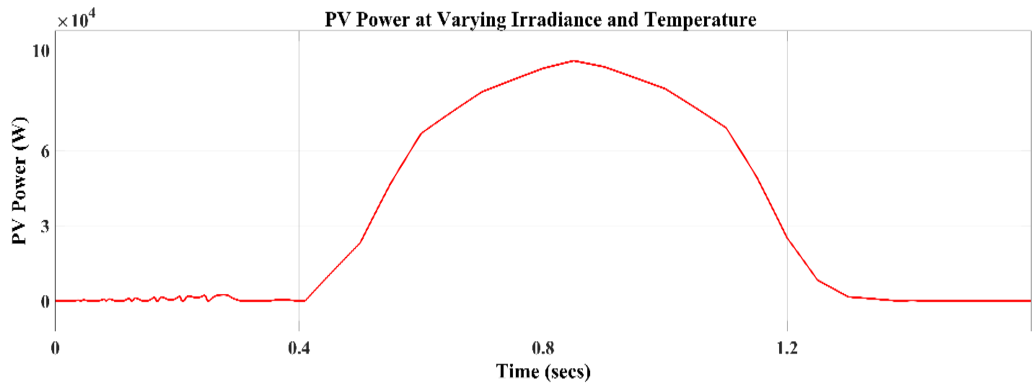


**Figure 31. PV Power at varying Irradiance and Temperature**

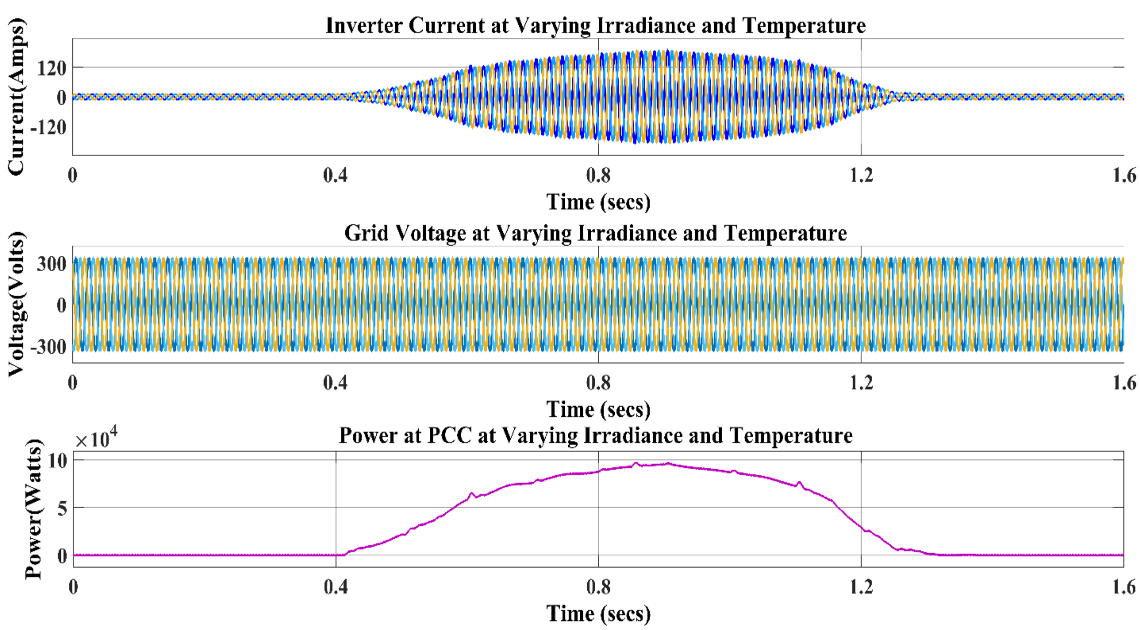


**Figure 32. Inverter Current, Grid Voltage and Power at PCC at Varying Irradiance and temperature.**

Figure (32) shows that at the Point of Common Coupling (PCC), power output varies with changes in irradiance and temperature. A slight reduction in power is observed due to the negative temperature coefficient of the PV modules, leading to a small decrease in overall power output.

Figure (33) depicts the capacitor current over 24 hours under varying irradiance and temperature. The current remains minimal, indicating the capacitor's primary role is stabilizing DC link voltage by smoothing transient variations, even during dynamic environmental changes

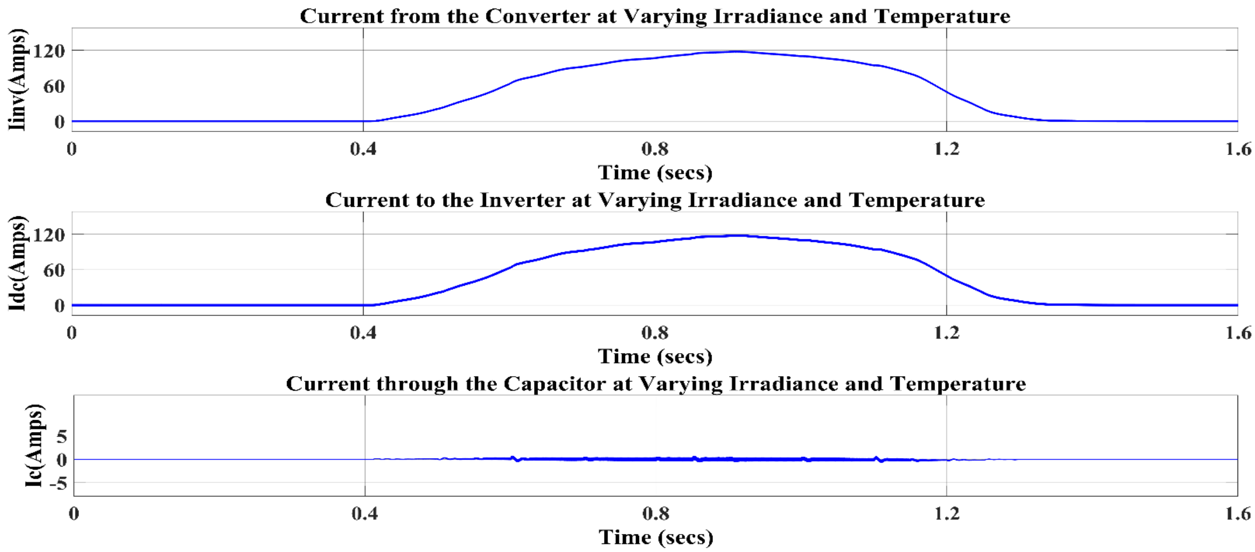


**Figure 33. Currents from the Converter, to the Inverter and through the Capacitor at Varying Irradiance and Temperature.**

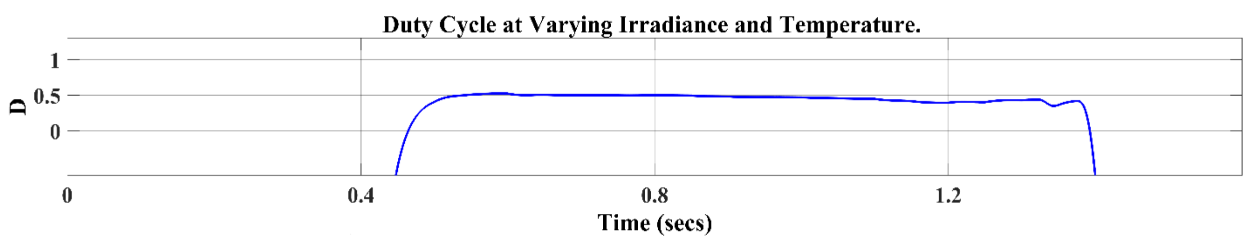


**Figure 34. Duty Cycle at Varying Irradiance and Temperature**

The figure (34) shows that the duty cycle remains consistently at 0.49, despite variations in irradiance and temperature. This indicates effective regulation by the control system, ensuring stable performance and efficient energy transfer, while minimizing the impact of environmental changes.

**Table 6. Power Values at Different Irradiance and Temperature**

| SL.NO. | Irradiance (w/m^2) | Temperature (°C) | Output of Module (KW) | Output of converter (KW) | At PCC (KW) |
|---|---|---|---|---|---|
| 1 | 1000 | 25 | 100 | 99.37 | 99.32 |
| 2 | 800 | 25 | 80.74 | 80.0 | 79.57 |
| 3 | 500 | 25 | 50.74 | 50.02 | 49.88 |
| 4 | 300 | 25 | 30.26 | 29.9 | 29.74 |
| 5 | 1000 | 35 | 93 | 92.25 | 92.18 |
| 6 | 1000 | 30 | 97 | 96.58 | 96.37 |
| 7 | 1000 | 25 | 99.88 | 99.81 | 99.30 |
| 8 | 1000 | 20 | 99.99 | 100 | 99.10 |
| 9 | 0 | 21 | 0 | 0 | 0 |
| 10 | 10 | 22 | 0 | 0 | 0 |
| 11 | 20 | 23 | 0 | 0 | 0 |
| 12 | 30 | 25 | 327 | 49 | 5.90 |
| 13 | 50 | 28 | 378 | 39 | 6.8 |
| 14 | 270 | 30 | 23.180 | 21.1460 | 20.210 |
| 15 | 700 | 32 | 62.890 | 58.300 | 57.540 |
| 17 | 970 | 34 | 92.750 | 87.730 | 86.930 |
| 18 | 1000 | 35 | 95.770 | 95.460 | 95.120 |
| 19 | 970 | 34 | 93.360 | 92.810 | 92.254 |
| 20 | 870 | 33 | 84.610 | 87.930 | 87.860 |
| 21 | 700 | 30 | 69.030 | 74.540 | 74.080 |
| 22 | 260 | 28 | 25.170 | 34.480 | 33.480 |
| 23 | 100 | 25 | 1.680 | 3.876 | 3.337 |
| 24 | 40 | 23 | 209 | 0 | 2.8 |
| 25 | 25 | 22 | 0 | 0 | 0 |
| 26 | 0 | 21 | 0 | 0 | 0 |

The table (6) shows the value of power at different irradiance and temperatures. From SL.NO. (1 to 4) gives the readings at constant temperature, SL.NO. (5 to 8) gives power for constant irradiance and SL.NO. (9 to 26) gives the power at diurnal irradiance and temperature variations.

### 4.6 Case 5: For Reactive Power Compensation.

During the absence of the PV, the STATCOM functions as reactive power provider. By incorporating a capacitor at the DC input as shown in figure (35), the inverter is configured to function as a reactive power source. However, fluctuations in the DC bus voltage, caused by capacitor charging and discharging, can affect reactive power stability. To address this, a series resistor is employed as a damping mechanism to regulate current flow and stabilize the DC bus voltage. This ensures consistent reactive power output and enhances the inverter's performance in grid support applications.

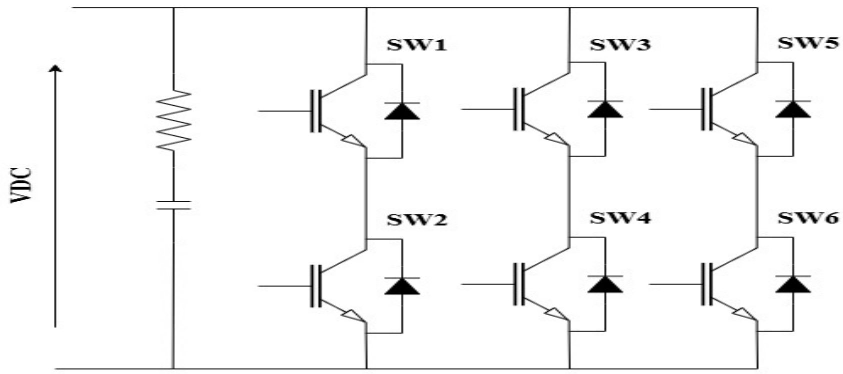


**Figure 35. Three Phase VSI**

The active power drawn from the grid is often influenced by the resistive losses in the system. As resistive losses increase (with higher resistance), the inverter compensates by drawing more active power and lower resistance reduces losses and grid power draw. The negative sign for active power indicates the direction of power flow. Power is being drawn from the grid to compensate system losses. For $R=10\times10^{-3}\ \Omega$ the grid supplies -187 W of active power to compensate for high resistive losses. For $R=0.1\times10^{-3}\ \Omega$ the resistive losses reduce significantly, and the active power demand drops to -56 W. This can be seen from the table (7).

**Table 7. Active Power Drawn and Reactive Power Supplied At Different Values of Resistance**

| Resistance value (ohms) | Active power drawn (Watts) | | Reactive power supplied (VAR) | |
|---|---|---|---|---|
| | Inverter output | At the grid | Inverter output | At the grid |
| 10e-3 | -190 | -139 | 1.09e+5 | 99.96e +3 |
| 5e-3 | -165 | -112 | 1.09e+5 | 99.96e +3 |
| 1e-3 | -153 | -98 | 1.09e+5 | 99.96e +3 |
| 0.5e-3 | -151 | -96 | 1.09e+5 | 99.96e +3 |
| 0.1e-3 | -142 | -86 | 1.09e+5 | 99.96e +3 |

According to IEEE 1547, mandates that distributed energy resources (DERs), such as photovoltaic (PV) systems equipped with STATCOM, must be capable of providing reactive power within a range that supports voltage regulation and grid stability. Specifically, the standard stipulates that the reactive power output should fall within a range of ±0.9 to ±0.95 of the system's rated active power capacity, ensuring that the system can contribute effectively to voltage control in the grid.

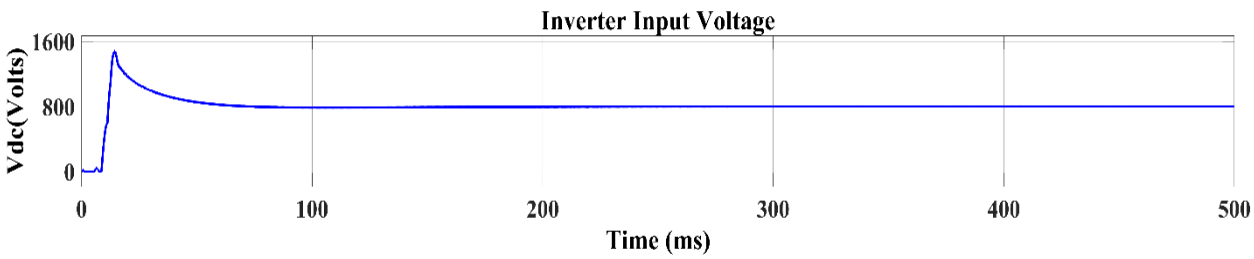


**Figure 36. Inverter Input Voltage**

The figure (36) shows the constant dc voltage of 800v maintained at the input capacitor of the inverter. This regulated DC voltage is essential for ensuring stable inverter functionality and facilitating efficient reactive power compensation, particularly during STATCOM operation in the absence of photovoltaic (PV) generation.

The figure (37) shows the reactive power supplied by the inverter to the grid in the absence of the photovoltaic system. The STATCOM, regulated by the controller, consistently maintains a reactive power output of 100 KVAR, while the active power remains at zero, ensuring efficient grid support under these conditions.

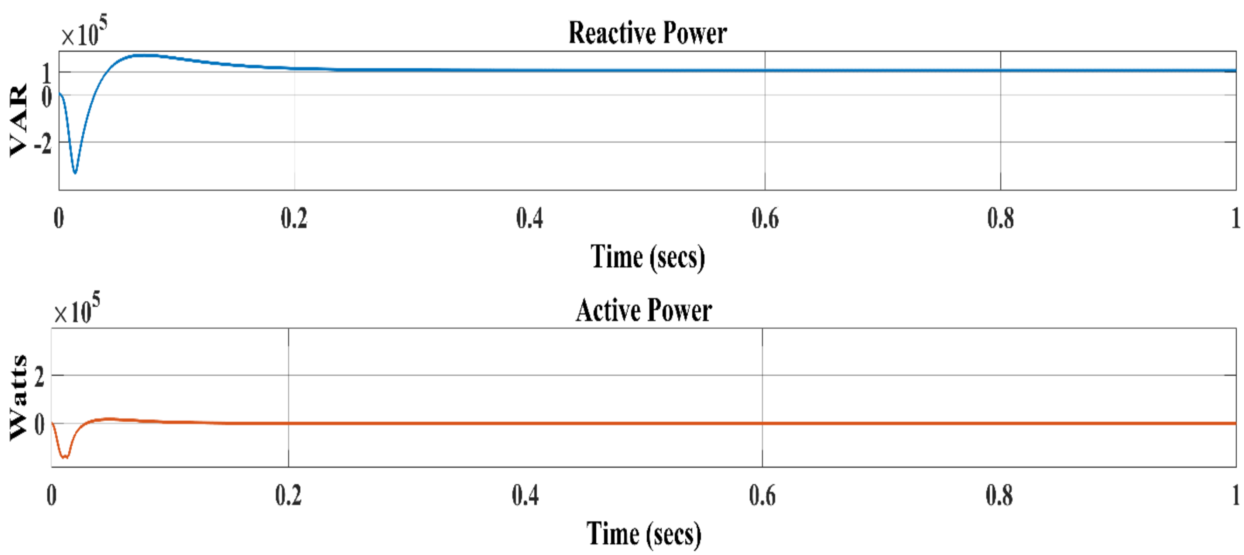


**Figure 37. Reactive Power and Active Power**

The figure (38) displays the voltage at the grid and the grid current after passing through the filter inverter, a phase difference is observed, with the voltage lagging the current, indicating the reactive power is from the inverter to the grid.

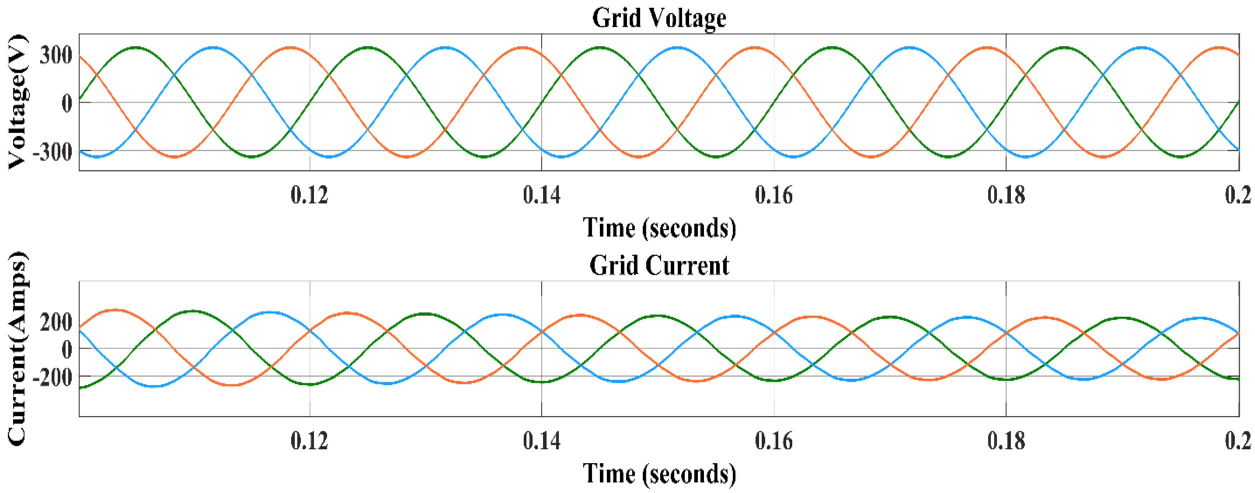


**Figure 38. Grid Voltage and Grid Current**

## 5. Conclusion:

The grid-connected PV system is simulated in MATLAB/SIMULINK, with analysis focusing on key parameters such as current, voltage, and power at various points: the module, the converter input, and the converter output. Additionally, the current through the capacitor at the inverter's input and the variations in the duty cycle with changes in temperature and irradiance are also evaluated. The system consistently maintains maximum power output, with minimal leakage current through the input capacitor. The DC input voltage of the inverter remains stable by the dynamic adjustment of the duty cycle through the ANFIS-based Maximum Power Point Tracking (MPPT) algorithm and the current controller. The system demonstrates low Total Harmonic Distortion (THD), ensuring efficient operation. In the absence of PV generation, the inverter functions as a reactive power compensator, with both active and reactive power being managed through the STATCOM, maintaining grid stability.

## References

[1] *M. Kumar and A. Singh, "Two Stage Power Conversion For Grid Connected PV Using Current Control Technique," Third International Conference on Intelligent Computing Instrumentation and Control Technologies (ICICICT), IEEE* ***(2022)***.

[2] *H. Xu, X. Wang, L. Huang, J. Qian and J. Lou, "Research on Two-Stage Three-Phase Photovoltaic Grid-Connected System with MPPT", 4th International Conference on Power and Renewable Energy (ICPRE),* ***(2019)***.

[3] *Varma, P. S., & Narayanan, G, "Space Vector PWM as a Modified Form of Sine-Triangle PWM for Simple Analog or Digital Implementation", IETE Journal of Research, 52(6), 435–449* ***(2006)***.

[4] *MLAKIĆ, Dragan; MAJDANDŽIĆ, Ljubomir; NIKOLOVSKI, Srete, "ANFIS Used as a Maximum Power Point Tracking Algorithm for a Photovoltaic System", International Journal of Electrical and Computer Engineering (IJECE)* ***(2018)***.

[5] *Hepzibah, A. & Premkumar, Dr.K, "ANFIS current–voltage controlled MPPT algorithm for solar powered brushless DC motor based water pump", Electrical Engineering* ***(2020)***.

[6] *Javed, Muhammad & Waleed, Aashir & Virk, Umar Siddique & Hassan, Syed, "Comparison of the Adaptive Neural-Fuzzy Interface System (ANFIS) based Solar Maximum Power Point Tracking (MPPT) with other Solar MPPT Methods", 1-5. 10.1109/INMIC50486.2020.9318178,* ***(2020)***.

*[7] Yap, Kah Yung & Sarimuthu, Charles & Lim, Joanne, "Artificial Intelligence Based MPPT Techniques for Solar Power System: A review", Journal of Modern Power Systems and Clean Energy **(2020)**.*

*[8] Ramesh, T. & Saravanan, R. & Sekar, S, "Analysis of ANFIS MPPT Controllers for Partially Shaded Stand Alone Photovoltaic System with Multilevel Inverter", IAES International Journal of Robotics and Automation (IJRA) **(2018)**.*

*[9] Chitransh, Apar & Kumar, Sachin,"The Different Type of MPPT Techniques for Photovoltaic System", Indian Journal of Engineering and Materials Sciences **(2021)**.*

*[10] Ali Omar Baba, Guangyu Liu, Xiaohui Chen,"Classification and Evaluation Review of Maximum Power Point Tracking Methods", Sustainable Futures, Volume 2 **(2020)**.*

*[11] Manikandan, K, Sivabalan, A, Sundar, R. and Surya, P, 2020, March. "A study of landsman, sepic and zeta converter by particle swarm optimization technique", 6th international conference on advanced computing and communication systems (ICACCS) (pp. 1035-1038), IEEE **(2020)**.*

*[12] Varsha R "Design and Simulation of Closed Loop DC/DC Synchronous SEPIC Converter using PID Feedback Controller", International Research Journal of Engineering and Technology (IRJET) Volume: 07 Issue: 07 **(2020)**.*

[13] *A. P. Murdan, I. Jahmeerbacus and S. Z. S. Hassen, "Modeling and Simulation of a STATCOM for reactive power control", 4th International Conference on Emerging Trends in Electrical, Electronic and Communications Engineering (ELECOM),* IEEE ***(2022)*.**

*[14] P. Kumar, U. Das and S. Chatterjee, "A brief study on control structure of grid connected PV inverter", International Conference on Energy Efficient Technologies for Sustainability (ICEETS) **(2016)**.*

*[15] CH Venkata Ramesh, A Manjunatha, "Compensation of Reactive Power in Grid- Connected Solar PV Array System Using STATCOM and Fixed Capacitor Bank",* International Journal of Engineering Trends and Technology*, vol. 69, no. 10, pp. 128-136 **(2021)**.*

*[16] Hava, Ahmet & Ayhan, Ufuk & Aban, Vahap, "A DC bus capacitor design method for various inverter applications", 2012 IEEE Energy Conversion Congress and Exposition, ECCE **2012**.*

*[17] Adamidis, Georgios & Tsengenes, G. & Kelesidis, K, Three Phase Grid Connected Photovoltaic System with Active and Reactive Power Control Using "Instantaneous Reactive Power Theory", Renewable Energy and Power Quality Journal, **(2010)**.*

*[18] Memon, Munwar, "Sizing of dc-link capacitor for a grid connected solar photovoltaic inverter", Indian Journal of Science and Technology, **(2020)**.*

*[19] Deshmukh, Shruti & Limkar, Shruti & Nagthane, Rushikesh & Pande, V.N. & Tare, Arti, "Design of Grid-Connected Solar PV System Integrated with Battery Energy Storage System", **(2023)**.*